UDC 519.61:624.074.4:624.04
Original scientific paper
Received: 13.03.2008.

Recent developments in nonlinear shell theory with finite rotations and finite deformations

Adnan Ibrahimbegović[(1)] and **Boštjan Brank**[(2)]
[(1)]Ecole Normale Superieure de Cachan, 61, Avenue du President Wilson, 94235 Cachan, FRANCE
e-mail: ai@lmt.ens-cachan.fr
[(2)]University of Ljubljana, Civil Engineering Department, Jamova 2, SI-1000 Ljubljana, SLOVENIA
e-mail: bostjan.brank@fgg.uni-lj.si

SUMMARY

In this paper we discuss a theoretical formulation of a fully nonlinear shell model, capable of representing finite rotations and finite strains. The latter imposes that one should account for through-the-thickness stretching, which allows for direct use of 3D constitutive equations from classical continuum model. Three different possibilities for implementing this kind of shell model within the framework of the finite element method are examined, the first one leading to 7 nodal parameters and the remaining two to 6 nodal parameters. The 7-parameter shell model with no simplification of kinematic terms is compared to the 7-parameter shell model which exploits usual simplifications of the Green-Lagrange strains. Two different ways of implementing the incompatible mode method for reducing the number of parameters to 6 are presented. One implementation uses an additive decomposition of the strains and the other an additive decomposition of the deformation gradient. A couple of numerical examples are given to illustrate performance of the shell elements developed herein.

***Key words**: shell, nonlinear shell model, finite rotations, finite deformations, addaptive decomposition.*

1. INTRODUCTION

The very recent research on the shell problem in the computational mechanics community is closing the gap between the classical shell model (which is basically 2D) and the classical 3D solid model [1]. While the latter was mastered long ago, the former - the nonlinear analysis of shells - has mainly been restricted to the shell models which are naturally placed within the theoretical framework of the Cosserat surface [2]. Even in such a simplified setting the numerical implementation issues have been finally settled fairly recently (see Ref. [3] for a recent review).

With both types of numerical models available it was natural to try to address an always present need to produce a model which would fit in between the shell (possibly retaining its computational efficiency) and the 3D solid.

A model of that kind can serve well in representing a stress variation in through-the-thickness direction, and eventual boundary layer effects. More importantly, it can directly use the 3D version of constitutive relations and thus eliminate eventual complexities stemming from imposing the zero-through-the-thickness-stress restriction on any constitutive model. It is desirable that such a shell model (further referred to as 3D shell) be capable of recovering the 2D shell behavior in the limit case of thin shell, as well as be considerably better in recovering true stress field for a thick shell than the usual thick shell model of Reissner-Mindlin type.

This paper is the extended version of the work presented at Special Workshop on Advanced Numerical Analysis of Shell-like Structures, Zagreb, Croatia, 2007 [1].

A few different approaches have been explored recently. The first group of works (Refs. [4-6]) started with the Reissner-Mindlin shell model (with three displacements of the mid-surface and two rotation parameters of the shell director typically used for smooth shells) enriching it further by a desired number of parameters to permit a reliable representation of through-the-thickness stretching. Those parameters are either independent kinematic variables, or strain variables constructed in the framework of the enhanced assumed strain (EAS) method, which are further eliminated at the finite element level. Second group (Refs. [7-9]) went along a similar path, but instead of describing shell director deformation with two rotation parameters they rather used three components of so-called difference vector. So developed shell models posses no rotation degrees of freedom. Final group to be mentioned (see Refs. [10-12]) preferred to take a solid element as the basis for their developments. They reduced the shell like features of the so developed elements to special treatment of shear deformation along with the modifications for through-the-thickness stretching.

For any of the 3D shell models mentioned above, the use of the fully 3D constitutive equations should preferably be accompanied by a linear variation of the through-the-thickness deformation component. This imposes 2 additional kinematic parameters for models with rotations and 1 for models with displacements only. One arrives at a 7-parameter shell theory. If one intends to decrease the computational efficiency and, more importantly, simplify the issues of the corresponding boundary conditions, the method of incompatible modes (see Refs. [13-15]) ought to be employed in order to reduce the number of parameters to 6.

We focus in this work on two questions. First, we study the difference between a 7-parameter theory where the exact expressions are used for the Green-Lagrange strain measures versus the shell theory where the usual simplifications are carried out by neglecting certain terms. The former of these two models can be developed without difficulty mostly for our use of symbolic manipulation. The second study is oriented towards two possible implementations of the method of incompatible modes: one with an additive decomposition of strains (Ref. [14]) versus the other with an additive decomposition of the deformation gradient which leads to a multiplicative decomposition of strains (Ref. [15]).

The outline of the paper is as follows. In Section 2 we lay the governing equations of the 7-parameter shell model. Two different variants of the incompatible mode methods are presented in Section 3. In Section 4 we provide some details of the numerical implementation. Several numerical examples are presented in Section 5 and the concluding remarks are given in Section 6.

2. SHELL THEORY WITH 7 PARAMETERS

In this section we first elaborate upon a shell formulation which employs the Reissner-Mindlin hypothesis that a straight fiber remains straight, but with enhanced, higher-order variation of the through-the-thickness displacement components. We then move on to develop the corresponding form of the Green-Lagrange strain measures. To complete the theory we deal with the simplest set of hyperelastic constitutive equations: the St.Venant-Kirchhoff and the neo-Hookean materials. Finally, the equilibrium equations are presented in their weak form along with their consistent linearization.

Contrary to the classical Reissner-Mindlin kinematics (incapable of accounting for through-thethickness deformation), we set to develop an enriched kinematic field in order to extend the potential application domain of the developed shell model. To that end, the shell position vector from the initial configuration:

$$\boldsymbol{x}_0\left(\xi^1,\xi^2,\zeta\right)=\varphi_0\left(\xi^1,\xi^2\right)+\zeta\frac{h_0}{2}\boldsymbol{g}\left(\xi^1,\xi^2\right) \quad (1)$$

with:

$$\|\boldsymbol{g}\|=1,\quad \left(\xi^1,\xi^2\right)\subset A\subset \mathbb{R}^2,\quad \zeta\in[-1,1] \quad (2)$$

(where ξ_1, ξ_2 and ζ are natural or convected coordinates, φ_0 is the position vector of the shell middle surface, h_0 is the initial constant shell thickness, A is the domain of the shell middle surface parametrization, and $\boldsymbol{g}$ is the initial unit normal or shell director) is transformed into its counterpart at the deformed configuration as:

$$\boldsymbol{x}\left(\xi^1,\xi^2,\zeta\right)=\varphi\left(\xi^1,\xi^2\right)+\zeta\frac{h\left(\xi^1,\xi^2\right)}{2}\boldsymbol{a}\left(\xi^1,\xi^2\right)+$$
$$+\left[\zeta\frac{h\left(\xi^1,\xi^2\right)}{2}\right]^2\tilde{q}\left(\xi^1,\xi^2\right)\boldsymbol{a}\left(\xi^1,\xi^2\right) \quad (3)$$

with:

$$\|\boldsymbol{a}\|=1 \quad (4)$$

and:

$$\varphi\left(\xi^1,\xi^2\right)=\varphi_0\left(\xi^1,\xi^2\right)+\boldsymbol{u}\left(\xi^1,\xi^2\right) \quad (5)$$

In Eqs. (3) and (5) $\boldsymbol{u}$ is the displacement vector providing a new position of the middle surface, h is current shell thickness, $\boldsymbol{a}$ is current position of the shell director and $\tilde{q}$ is the hierarchical term introducing the displacement quadratic variation in the through-the-thickness direction. Considering that we allow for thickness change in the direction of ζ coordinate (note that ζ coordinate is not perpendicular to the middle surface at the deformed configuration) with:

$$\lambda\left(\xi^1,\xi^2\right)=\frac{h\left(\xi^1,\xi^2\right)}{h_0} \tag{6}$$

we may write Eq. (3) as:

$$\boldsymbol{x}\left(\xi^1,\xi^2,\zeta\right)=\boldsymbol{\varphi}\left(\xi^1,\xi^2\right)+\zeta\frac{h_0}{2}\lambda\left(\xi^1,\xi^2\right)\boldsymbol{a}\left(\xi^1,\xi^2\right)+ \\ +\zeta^2\frac{{h_0}^2}{2}q\left(\xi^1,\xi^2\right)\boldsymbol{a}\left(\xi^1,\xi^2\right) \tag{7}$$

where:

$$q=\lambda\tilde{q} \tag{8}$$

We note that the structure of the term for quadratic variation of displacements in through-the-thickness direction chosen in Eq. (7) is just one of several possibilities. To simplify the notation we further rewrite Eq. (7) as (this equation can be regarded as a two-term approximation of equation $\boldsymbol{x}=\boldsymbol{\varphi}+\sum_{n=1}^{\infty}\zeta^n\boldsymbol{d}_n$ given by Ref. [2] (page 466) to derive a shell theory from the 3D solid; see also Ref. [16]):

$$\boldsymbol{x}\left(\xi^1,\xi^2,\zeta\right)=\boldsymbol{\varphi}\left(\xi^1,\xi^2\right)+\zeta\boldsymbol{d}\left(\xi^1,\xi^2\right)+\zeta^2\boldsymbol{f}\left(\xi^1,\xi^2\right) \tag{9}$$

where:

$$\boldsymbol{d}=\frac{h_0}{2}\lambda\boldsymbol{a},\quad \boldsymbol{f}=\frac{{h_0}^2}{4}q\boldsymbol{a} \tag{10}$$

The position of the shell director $\boldsymbol{a}$ is defined by two rotational parameters, which are in this work two components of the total material rotation vector ϑ:

$$\boldsymbol{a}=\boldsymbol{a}(\vartheta^1,\vartheta^2) \tag{11}$$

(see Ref. [17] or Ref. [18] for details). The configuration space consistent with the choice of kinematics indicated in Eq. (3) has 7 parameters:

$$C=\left\{\begin{array}{l|l}\boldsymbol{\Phi}=\left(\varphi,a,\lambda,q\right) & A\to\mathbb{R}^3\times S^2\times\mathbb{R}^+\times\mathbb{R} \\ \varphi_{|\partial\varphi A}=\bar{\varphi},\boldsymbol{a}_{|\partial aA}=\bar{\boldsymbol{a}},\lambda_{|\partial\lambda A}=\bar{\lambda},q_{|\partial qA}=\bar{q} & \end{array}\right\} \tag{12}$$

where $\partial\varphi A$, ... ∂qA are parts of the shell boundary where the corresponding variable value is prescribed. In Eq. (12), it is indicated that the unit vector $\boldsymbol{a}$ belongs to a unit sphere manifold, which imposes a special treatment of finite rotations (see Ref. [19] or Ref. [17]).

Departing from the classical exposition on the subject (Ref. [2]), which reduces the shell theory to a 2D setting, we keep herein the fully 3D picture. Consequently, the choice of the coordinates in the shell deformed configuration leads to the following vector basis:

$$\boldsymbol{a}_\alpha=\frac{\partial\boldsymbol{x}}{\partial\xi^\alpha}=\boldsymbol{\varphi}_{,a}+\zeta\boldsymbol{d}_{,\alpha}+\zeta^2\boldsymbol{f}_{,\alpha} \\ \boldsymbol{a}_3=\frac{\partial\boldsymbol{x}}{\partial\zeta}=\boldsymbol{d}+2\zeta\boldsymbol{f} \tag{13}$$

where $(o)_{,\alpha}=\frac{\partial(o)}{\partial\xi^\alpha}$, α = *1, 2* and:

$$\boldsymbol{d}_{,\alpha}=\frac{h_0}{2}\left(\lambda_{,\alpha}\boldsymbol{a}+\lambda\boldsymbol{a}_{,\alpha}\right),\quad \boldsymbol{f}_{,\alpha}=\frac{{h_0}^2}{4}\left(q_{,\alpha}\boldsymbol{a}+q\boldsymbol{a}_{,\alpha}\right) \tag{14}$$

The Green-Lagrange strains may be written as:

$$\boldsymbol{E}=\frac{1}{2}\left(\boldsymbol{F}^T\boldsymbol{F}-\boldsymbol{1}\right)=\frac{1}{2}\left(\boldsymbol{C}-\boldsymbol{1}\right)=E_{ij}\boldsymbol{g}^i\otimes\boldsymbol{g}^j \tag{15}$$

where $\boldsymbol{F}$ is deformation gradient, $\boldsymbol{1}$ is unit tensor, $\boldsymbol{C}$ is right Cauchy-Green stretch tensor and $\boldsymbol{g}^i$ are contravariant base vectors of the initial configuration, defined as $\boldsymbol{g}_i\cdot\boldsymbol{g}_j=\delta_i{}^j$, where $\delta_i{}^j$ is Kronecker delta symbol. Base vectors $\boldsymbol{g}_i$ follow from Eq. (1) as:

$$\boldsymbol{g}_\alpha=\frac{\partial\boldsymbol{x}_0}{\partial\xi^\alpha}=\boldsymbol{\varphi}_{0,a}+\zeta\frac{h_0}{2}\boldsymbol{g}_{,\alpha} \\ \boldsymbol{g}_3=\frac{\partial\boldsymbol{x}_0}{\partial\zeta}=\frac{h_0}{2}\boldsymbol{g} \tag{16}$$

Note that $\boldsymbol{g}^3=2\boldsymbol{g}/h_0$. Strains in that basis are defined as ($\boldsymbol{F}=\boldsymbol{a}_i\otimes\boldsymbol{g}^i$ and $\boldsymbol{1}=\boldsymbol{g}_i\cdot\boldsymbol{g}_j\,\boldsymbol{g}^i\otimes\boldsymbol{g}^j$):

$$E_{ij}=\frac{1}{2}\left(\boldsymbol{a}_i\cdot\boldsymbol{a}_j-\boldsymbol{g}_i\cdot\boldsymbol{g}_j\right)= \\ =H_{ij}+\zeta K_{ij}+\zeta^2L_{ij}+\zeta^3M_{ij}+\zeta^4N_{ij} \tag{17}$$

with their explicit forms (note that the through-the-thickness coordinate in shell theories is usually defined as $\xi=\zeta\frac{h_0}{2}$ having $(o)_3=\frac{\partial(o)}{\partial\xi}$. Since we work here with ζ coordinate and $(o)_3=\frac{\partial(o)}{\partial\zeta}$, we obtain for strains an additional term of $\frac{h_0}{2}$ for each subscript 3) can be obtained by using Eqs. (13) and (16):

$$H_{\alpha\beta}=\frac{1}{2}\left(\varphi_{,\alpha}\cdot\varphi_{,\beta}-\varphi_{0,\alpha}\cdot\varphi_{0,\beta}\right) \\ H_{\alpha3}=\frac{1}{2}\left(\varphi_{,\alpha}\cdot\boldsymbol{d}-\frac{h_0}{2}\underbrace{\varphi_{0,\alpha}\cdot\boldsymbol{g}}_{0}\right) \\ H_{33}=\frac{1}{2}\left(\boldsymbol{d}\cdot\boldsymbol{d}-\frac{h_0}{4}\right) \tag{18}$$

$$K_{\alpha\beta}=\frac{1}{2}\left(\varphi_{,\alpha}\cdot\boldsymbol{d}_{,\beta}-\varphi_{,\beta}\cdot\boldsymbol{d}_{,\alpha}-\frac{h_0}{2}\varphi_{0,\alpha}\cdot\boldsymbol{g}_{,\beta}-\frac{h_0}{2}\varphi_{0,\beta}\cdot\boldsymbol{g}_{,\alpha}\right) \\ K_{\alpha3}=\frac{1}{2}\left(\boldsymbol{d}_{,\alpha}\cdot\boldsymbol{d}+2\varphi_{,\alpha}\cdot\boldsymbol{f}-\frac{h_0^2}{4}\underbrace{\boldsymbol{g}_{0,\alpha}\cdot\boldsymbol{g}}_{0}\right) \\ K_{33}=\frac{1}{2}\left(4\boldsymbol{f}\cdot\boldsymbol{d}\right) \tag{19}$$

$$L_{\alpha\beta} = \frac{1}{2}\left(\boldsymbol{d}_{,\alpha} \cdot \boldsymbol{d}_{,\beta} + \varphi_{,\alpha} \cdot \boldsymbol{f}_{,\beta} + \varphi_{,\beta} \cdot \boldsymbol{f}_{,\alpha} - \frac{h_0}{4} \boldsymbol{g}_{,\alpha} \cdot \boldsymbol{g}_{,\beta} \right)$$

$$L_{\alpha 3} = \frac{1}{2}\left(2\boldsymbol{d}_{,\alpha} \cdot \boldsymbol{f} + \boldsymbol{f}_{,\alpha} \cdot d \right) \qquad (20)$$

$$L_{33} = \frac{1}{2}\left(4\boldsymbol{f} \cdot \boldsymbol{f} \right)$$

$$M_{\alpha\beta} = \frac{1}{2}\left(\boldsymbol{d}_{,\alpha} \cdot \boldsymbol{f}_{,\beta} + \boldsymbol{d}_{,\beta} \cdot \boldsymbol{f}_{,\alpha} \right)$$

$$M_{\alpha 3} = \frac{1}{2}\left(2\boldsymbol{f}_{,\alpha} \cdot \boldsymbol{f} \right) \qquad (21)$$

$$M_{33} = 0$$

$$N_{\alpha\beta} = \frac{1}{2}\left(\boldsymbol{f}_{,\alpha} \cdot \boldsymbol{f}_{,\beta} \right)$$

$$N_{\alpha 3} = 0 \qquad (22)$$

$$N_{33} = 0$$

From the above expressions it can be seen that the in-plane shell strains are of fourth order with respect to ζ coordinate, while the transverse shear strains and the transverse normal strain vary cubically and quadratically, respectively.

Usual simplification carried out in the shell theory developments (see Refs. [9, 20, 21]) is to truncate expression (17) after the linear term, so that:

$$E_{ij} \rightarrow H_{ij} + \zeta K_{ij} \qquad (23)$$

In this work we will develop a model with exact expressions for strains and a simplified model with constant and linear variation of strains through the thickness.

Having defined the kinematics for the chosen 7-parameter shell model, we proceed with the constitutive equations. We will restrict ourself to a simplest set of hyperelastic materials: the St.Venant-Kirchhoff and the neo-Hookean. The stored energy density function per unit initial volume of the St.Venant-Kirchhoff material is defined as:

$$W\left(\boldsymbol{E}\right) = \frac{\lambda}{2}\left(tr\ \boldsymbol{E}\right)^2 + \mu\, tr\ \boldsymbol{E}^2 \qquad (24)$$

where $\lambda = \dfrac{E\nu}{(1+\nu)(1-2\nu)}$ and $\mu = \dfrac{E}{2(1+\nu)}$ are Lame coefficients, $tr(o)$ is trace of tensor (o), and $\boldsymbol{E}$ is the Green-Lagrange strain tensor deduced above. The stored energy density function for the neo-Hookean material reads as:

$$W\left(\boldsymbol{E}\right) = \frac{\lambda}{2}\left(J-1\right)^2 + \mu\left(\frac{tr\,\boldsymbol{C} - 3}{2} - \ln J \right) \qquad (25)$$

where $J = \sqrt{det\,\boldsymbol{C}}$. No shear correction factors are used in the constitutive models. Derivation of Eqs. (24) and (25) with respect to the strain tensor leads to expressions for the *2nd* Piola-Kirchhoff stress tensor. So, we have:

$$\boldsymbol{S} = \frac{\partial W}{\partial \boldsymbol{E}} = \lambda\ tr\ \boldsymbol{E}\boldsymbol{1} + 2\mu\boldsymbol{E} = S^{ij}\boldsymbol{g}_i \otimes \boldsymbol{g}_j \qquad (26)$$

for the St.Venant-Kirchhoff material and:

$$\boldsymbol{S} = 2\frac{\partial W}{\partial \boldsymbol{C}} = \lambda\left(J-1\right)J\boldsymbol{C}^{-1} + \mu\left(\boldsymbol{1} - \boldsymbol{C}^{-1}\right) = S^{ij}\boldsymbol{g}_i \otimes \boldsymbol{g}_j \qquad (27)$$

for the neo-Hookean material. Derivation of stresses with respect to strains gives the components of the constitutive tensor:

$$C = \frac{\partial \boldsymbol{S}}{\partial \boldsymbol{E}} = \frac{\partial^2 W\left(\boldsymbol{E}\right)}{\partial \boldsymbol{E}^2} = C^{ijkl}\boldsymbol{g}^i \otimes \boldsymbol{g}^j \otimes \boldsymbol{g}^k \otimes \boldsymbol{g}^l \qquad (28)$$

We can thus write the total potential energy for the present shell model in the same way as for the 3D solid:

$$\Pi\left(\varphi, a, \lambda, q\right) = \int_A \int_{h_0} W\left[\boldsymbol{E}\left(\varphi, a, \lambda, q\right)\right] dV + \Pi_{ext}\left(\varphi\right) \qquad (29)$$

where A defines the shell middle surface and Π_{ext} is the potential of the conservative external forces acting on the middle surfaces (note that the potential of the conservative external forces can be extended to the forces acting on the shell top and bottom surfaces, i.e. $\Pi_{ext} = \Pi_{ext}\left(\varphi + \zeta\boldsymbol{d} + \zeta^2\boldsymbol{f}\right)$, where $\zeta = \pm 1$) of the shell, which may be written as:

$$\Pi_{ext}\left(\varphi\right) = -\int_A h_0\rho_0\bar{\boldsymbol{b}} \cdot \varphi dA - \int_A \boldsymbol{p} \cdot \varphi dA - \int_{\partial A} \bar{\boldsymbol{t}} \cdot \varphi ds \qquad (30)$$

In Eq. (30) $\bar{\boldsymbol{b}}$, $\boldsymbol{p}$ and $\bar{\boldsymbol{t}}$ are applied body forces, pressure forces and forces acting on the edges of the shell middle-surface, respectively, and ρ_0 is the initial 3D mass density. Variation of Eq. (29) with respect to the independent kinematic variables leads to the weak form of equilibrium equations:

$$\int_A \int_{h_0} \frac{\partial W\left(\boldsymbol{E}\right)}{\partial \boldsymbol{E}} \partial\boldsymbol{E}\partial V = D\Pi_{ext}\left(\varphi\right) \cdot \partial\varphi \qquad (31)$$

where the variation of strains, $\delta\boldsymbol{E} = D\boldsymbol{E}(\boldsymbol{\Phi}) \cdot \delta\boldsymbol{\Phi}$ can be obtained by varying Eqs. (18) to (22). Linearization of Eq. (31) gives the tangent operator:

$$\int_A \int_{h_0} \left[\left(C\Delta\boldsymbol{E}\right)\delta\boldsymbol{E} + \boldsymbol{S}\left(\Delta\delta\boldsymbol{E}\right) \right] dV \qquad (32)$$

where $\Delta\boldsymbol{E}$ is the linearization of strains $\Delta\boldsymbol{E} = D\boldsymbol{E}(\boldsymbol{\Phi}) \cdot \delta\boldsymbol{\Phi}$, and $\Delta\delta\boldsymbol{E}$ is the linearization of the variation of strains $\Delta\delta\boldsymbol{E} = D[\delta\boldsymbol{E}(\boldsymbol{\Phi})] \cdot \Delta\boldsymbol{\Phi}$.

3. SHELL THEORY WITH 6 PARAMETERS AND INCOMPATIBLE MODES

The 7-parameter shell theory developed in the previous section is very much geared towards the applications of a shell-like structures, and it might be difficult to use it as a part of the model of a complex system. Therefore, we develop in this section an alternative implementation of the shell theory with through-the-thickness stretching where the number of parameters is reduced to 6, which might be easier to combine with solids. In order to accommodate the linear variation of the through-the-thickness stretch we resort to the method of incompatible modes. We obtain a shell finite element with 6 nodal parameters, which possesses an additional advantage of fitting easier into the standard finite element software architecture.

Two possible implementations of the incompatible mode method are considered: one with an additive decomposition of strains and the other with an additive decomposition of the deformation gradient, which leads to a multiplicative decomposition of strains. The former is simpler, but only acceptable for small strains, whereas the latter, although more complex to handle, is also applicable for large strains.

3.1 Incompatible modes based on an additive decomposition of strains

If one wants to recover a 6-parameter (note that the same notation is used in sections 2 and 3, although some quantities of the 6-parameter shell theory (like $\boldsymbol{x}$, $\boldsymbol{a}_i$, some strains, etc.) are of different form than those of the 7-parameter shell theory) shell theory, the through-the-thickness displacement variation ought not be more than linear. This results in the following deformed configuration position vector:

$$\begin{aligned}\boldsymbol{x}\left(\xi^1,\xi^2,\zeta\right) &= \varphi\left(\xi^1,\xi^2\right)+\zeta\frac{h_0}{2}\lambda\left(\xi^1,\xi^2\right)\boldsymbol{a}\left(\xi^1,\xi^2\right)\\ &= \varphi\left(\xi^1,\xi^2\right)+\varsigma\boldsymbol{d}\left(\xi^1,\xi^2\right)\end{aligned} \tag{33}$$

with $\boldsymbol{d}$ already defined in Eq. (10). The corresponding base vectors are then:

$$\begin{aligned}\boldsymbol{a}_\alpha &= \frac{\partial\boldsymbol{x}}{\partial\xi^a}=\varphi_{,a}+\zeta\boldsymbol{d}_{,\alpha}\\ \boldsymbol{a}_3 &= \frac{\partial\boldsymbol{x}}{\partial\zeta}=\boldsymbol{d}\end{aligned} \tag{34}$$

The initial configuration position vector and its derivatives remain the same as indicated in Eqs. (1) and (16), respectively.

The configuration space of the shell model consistent with the choice of kinematics indicated in Eq. (33) has 6 parameters: 3 displacements of the middle surface, 2 rotation parameters defining the position of the shell director $\boldsymbol{a}$ and 1 through-the-thickness stretching parameter λ. It can be written as:

$$C=\left\{\begin{array}{c}\Phi=\left(\varphi,a,\lambda,\right)\Big|A\to\mathbb{R}^3\times S^2\times\mathbb{R}^+\Big|\\ \varphi_{|\partial\varphi A}=\bar{\varphi},\boldsymbol{a}_{|\partial aA}=\bar{\boldsymbol{a}},\lambda_{|\partial\lambda A}=\bar{\lambda}\end{array}\right\} \tag{35}$$

The Green-Lagrange strains for the 6-parameter model in the $\boldsymbol{g}^i$ base are then:

$$E_{ij}=\frac{1}{2}\left(\boldsymbol{a}_i\cdot\boldsymbol{a}_j-\boldsymbol{g}_i\cdot\boldsymbol{g}_j\right)=H_{ij}+\zeta K_{ij}+\zeta^2L_{ij} \tag{36}$$

where:

$$\begin{aligned}H_{\alpha\beta}&=\frac{1}{2}\left(\varphi_{,\alpha}\cdot\varphi_{,\beta}-\varphi_{0,\alpha}\cdot\varphi_{0,\beta}\right)\\ H_{\alpha3}&=\frac{1}{2}\left(\varphi_{,\alpha}\cdot\boldsymbol{d}\right)\\ H_{33}&=\frac{1}{2}\left(\boldsymbol{d}\cdot\boldsymbol{d}-\frac{h_0^2}{4}\right)\end{aligned} \tag{37}$$

$$\begin{aligned}K_{\alpha\beta}&=\frac{1}{2}\left(\varphi_{,\alpha}\cdot\boldsymbol{d}_{,\beta}+\varphi_{,\beta}\cdot\boldsymbol{d}_{,\alpha}-\frac{h_0}{2}\varphi_{0,\alpha}\cdot\boldsymbol{g}_{,\beta}-\frac{h_0}{2}\varphi_{0,\beta}\cdot\boldsymbol{g}_{,\alpha}\right)\\ K_{\alpha3}&=\frac{1}{2}\left(\boldsymbol{d}_{,\alpha}\cdot\boldsymbol{d}\right)\\ K_{33}&=0\end{aligned} \tag{38}$$

$$\begin{aligned}L_{\alpha\beta}&=\frac{1}{2}\left(\boldsymbol{d}_{,\alpha}\cdot\boldsymbol{d}_{,\beta}-\frac{h_0^2}{4}\boldsymbol{g}_{,\alpha}\cdot\boldsymbol{g}_{,\beta}\right)\\ L_{\alpha3}&=0\\ L_{33}&=0\end{aligned} \tag{39}$$

Through-the-thickness variation of the in-plane strains, the transverse shear strains and the transverse normal strain is quadratic, linear and constant, respectively. A problem arises from the zero value of K_{33} in Eq. (38), which implies a constant value of E_{33} strain. Namely, even for the simplest stress state of pure bending (equivalent to the patch test condition, see Ref. [22]) with the linear variation of in-plane strain components in through-the-thickness direction, the plane stress state can never be reproduced for any non-zero value of Poisson's ratio, since:

$$S^{33}=C^{33\alpha\beta}\underbrace{E_{\alpha\beta}}_{\text{linear in }\zeta}+C^{3333}\underbrace{E_{33}}_{\text{constant in }\zeta} \tag{40}$$

This kind of problem is often referred to as the Poisson's ratio stiffening (see Refs. [7, 23]).

If one would like to employ a 3D constitutive model for shells and still avoid the Poisson's ratio stiffening, it is indispensable to use a linear variation of the E_{33} strain component, which can be introduced by the incompatible mode method:

$$E_{ij} \to E_{ij} + \tilde{E}_{ij}, \quad \tilde{E}_{ij} = \begin{cases} 0 & i,j = 1 \text{ or } 2 \\ 0 & i \text{ or } j = 3 \\ \zeta\, A_{33} & i,j = 3 \end{cases} \quad (41)$$

This modification can then be introduced into the energy functional governing the shell problem according to:

$$\Pi\left(\underbrace{\varphi,\alpha,\lambda}_{\boldsymbol{\Phi}},\tilde{E}_{ij},S^{ij}\right) = \int\limits_{A}\int\limits_{h_0}\left\{\frac{1}{2}\left(E_{ij}+\tilde{E}_{ij}\right)C^{ijkl}\left(E_{kl}+\tilde{E}_{kl}\right) - S^{ij}\tilde{E}_{ij}\right\}dV - \Pi_{ext}(\varphi) \quad (42)$$

The second term in the integral in Eq. (42) represents the Lagrange multiplier modification forcing the enhancement $\tilde{E}_{33}$ to disappear in the strong form of the problem. The same does not happen in the weak form, which can be written as:

$$D\Pi\left(\boldsymbol{\Phi},\tilde{E}_{ij},S^{ij}\right)\cdot\delta\boldsymbol{\Phi} = \int\limits_{A}\int\limits_{h_0}\delta E_{ij}C^{ijkl}\left(E_{kl}+\tilde{E}_{kl}\right)dV - D\Pi_{ext}(\varphi)\delta\varphi = 0 \quad (43)$$

$$D\Pi\left(\boldsymbol{\Phi},\tilde{E}_{ij},S^{ij}\right)\cdot\delta\tilde{E}_{ij} = \int\limits_{A}\int\limits_{h_0}\delta\tilde{E}_{ij}\left[-S^{ij}+C^{ijkl}\left(E_{kl}+\tilde{E}_{kl}\right)\right]dV = 0 \quad (44)$$

$$D\Pi\left(\boldsymbol{\Phi},\tilde{E}_{ij},S^{ij}\right)\cdot\delta S_{ij} = \int\limits_{A}\int\limits_{h_0}\delta S^{ij}\tilde{E}_{ij}dV = 0 \quad (45)$$

Expressions (43) to (45) can be simplified by assuming orthogonality of the chosen strain enhancement and the stress field, making the first term in each of the last two equations to disappear. Eq. (45) implies that one should have:

$$0 = \int\limits_{A}\int\limits_{h_0}S^{33}\tilde{E}_{33}dV = \int\limits_{A}\int\limits_{h_0}S^{33}\left(\zeta A^{33}\right)dV \quad (46)$$

if $S^{33} = f\,unct\,(\xi^1,\xi^2)$.

One has to ensure, however, that the constant through-the-thickness stress field is contained in the chosen stress variation thus ensuring the patch test condition (Ref. [22]) in the following form:

$$\int\limits_{\square}\int\limits_{-1}^{1}\tilde{E}_{33}\underbrace{j\,d\zeta\,d\xi^1 d\xi^2}_{dV} = 0 \quad (47)$$

where $\square$ is a bi-unit square and j is Jacobian of the transformation from the initial shell finite element configuration to a bi-unit cube ($j = \sqrt{det\left[\boldsymbol{g}_i\cdot\boldsymbol{g}_j\right]}$).

Interpolation of A_{33} over the finite element may be chosen as:

$$A_{33}\left(\xi^1,\xi^2\right) = \frac{j_0}{j}\left(\alpha_1+\alpha_2\xi^1+\alpha_3\xi^2+\alpha_4\xi^1\xi^2\right) = \frac{j_0}{j}\boldsymbol{n}^T\boldsymbol{\alpha} \quad (48)$$

or otherwise with the bi-linear functions as:

$$A_{33}\left(\xi^1,\xi^2\right) = \frac{j_0}{j}\left[\hat{\alpha}_1 N_1\left(\xi^1,\xi^2\right)+\hat{\alpha}_2 N_2\left(\xi^1,\xi^2\right)+\hat{\alpha}_3 N_3\left(\xi^1,\xi^2\right)+\hat{\alpha}_4 N_4\left(\xi^1,\xi^2\right)\right] = \frac{j_0}{j}\hat{\boldsymbol{n}}^T\hat{\boldsymbol{\alpha}} \quad (49)$$

In Eqs. (48) and (49) j_0 is Jacobian at the center of the finite element (at $\xi_1=\xi_2=\zeta=0$), vector:

$$\boldsymbol{\alpha} = \left\{\alpha_1,\alpha_2,\alpha_3,\alpha_4\right\}^T \quad (50)$$

is vector of four local element strain parameters (note that in the following the procedures will be developed for $\boldsymbol{\alpha}$ parameters although they are also valid for $\tilde{\boldsymbol{\alpha}}$ parameters) associated with interpolation of $\tilde{E}_{33}$, and $\boldsymbol{n}$ is vector of interpolation functions for $\boldsymbol{\alpha}$. N_a (with $a=1,2,3,4$) are standard bi-linear interpolation functions for 4-node finite element (which is also a particular choice for the implementation of the present shell theory; see section 4):

$$N_a = \frac{1}{4}\left(1+\xi_a^1\xi^1\right)\left(1+\xi_a^2\xi^2\right), \quad \xi_a^1 \in \left[-1,1,1-1\right], \quad \xi_a^2 \in \left[-1,-1,1-1\right] \quad (51)$$

Equation (46) can be now exactly verified for constant S^{33} stress with respect to ζ coordinate, while from Eq. (47) it follows:

$$\underbrace{j_0\int\limits_{\square}\boldsymbol{n}\,d\xi^1 d\xi^2}_{0}\underbrace{\int\limits_{-1}^{1}\zeta\,d\zeta}_{0} = 0 \quad (52)$$

The set of remaining equations in (45) is highly nonlinear and ought to be handled by an iterative procedure. If the Newton method is used for such a purpose, one employs constant linearization of Eq. (45). The latter can easily be carried out by symbolic manipulation (see Ref. [24]). Implementation of the theory presented above in this section can be done by replacing the energy functional governing the shell problem (42) with four functionals, which have the following forms when defined over the finite element domain:

$$\Pi_{11}(\boldsymbol{\Phi}) = \frac{1}{2}\int\limits_{\square}\int\limits_{-1}^{1}E_{ij}C^{ijkl}E_{kl}\,j\,d\zeta\,d\xi^1 d\xi^2 - \Pi_{ext}(\varphi) \quad (53)$$

$$\Pi_{12}(\boldsymbol{\Phi},\alpha) = \frac{1}{2}\int\limits_{\square}\int\limits_{-1}^{1}E_{ij}C^{ijkl}\tilde{E}_{kl}\,j\,d\zeta\,d\xi^1 d\xi^2 \quad (54)$$

$$\Pi_{21}(\boldsymbol{\Phi},\alpha)=\frac{1}{2}\int_{\Omega}\int_{-1}^{1}\tilde{E}_{ij}C^{ijkl}E_{kl}\,j\,d\zeta\,d\xi^1 d\xi^2 \tag{55}$$

$$\Pi_{22}(\alpha)=\frac{1}{2}\int_{\Omega}\int_{-1}^{1}\tilde{E}_{ij}C^{ijkl}\tilde{E}_{kl}\,j\,d\zeta\,d\xi^1 d\xi^2 \tag{56}$$

Variation and linearization of Eqs. (53) to (55) carried out by symbolic manipulation with respect to the unknown quantities $\boldsymbol{\Phi} = (\varphi, \boldsymbol{a}, \lambda)$ and α provide the following set of linear equations:

$$\begin{Bmatrix}\delta\boldsymbol{\Phi}\\ \delta\alpha\end{Bmatrix}^T\left(\begin{bmatrix}\boldsymbol{K} & \tilde{\boldsymbol{F}}^T\\ \tilde{\boldsymbol{F}} & \tilde{\boldsymbol{H}}\end{bmatrix}\begin{Bmatrix}\delta\boldsymbol{\Phi}\\ \Delta\alpha\end{Bmatrix}=\begin{Bmatrix}\tilde{\boldsymbol{f}}\\ \boldsymbol{0}\end{Bmatrix}-\begin{Bmatrix}\tilde{\boldsymbol{r}}\\ \tilde{\boldsymbol{h}}\end{Bmatrix}\right) \tag{57}$$

where $\delta(o)$ are admissible variations, $\Delta(o)$ are linearized quantities, while matrices and vectors in Eq. (57) follow from the variation and linearization of Eqs. (53) to (56).The subsequent solution procedure follows along with the lines traced by Ref. [14].

3.2 Incompatible modes based on a multiplicative decomposition of strains

An alternative manner to introduce the incompatible modes is at the level of an additive decomposition of the deformation gradient, which would result in the corresponding multiplicative decomposition of strains (see Ref. [15]). In the present case the incompatible modes choice is dictated by the goal to achieve a linear variation in the through-the-thickness direction.

We replace the base vector $\boldsymbol{a}_3$ of the 6-parameter shell model, defined in previous section in Eq. (34), by a base vector $\bar{\boldsymbol{a}}_3$ of the following form:

$$\bar{\boldsymbol{a}}_3\left(\xi^1,\xi^2,\zeta\right)=\underbrace{\boldsymbol{d}\left(\xi^1,\xi^2\right)}_{\boldsymbol{a}_3\left(\xi^1,\xi^2\right)}+\tilde{\boldsymbol{b}}\left(\xi^1,\xi^2,\zeta\right) \tag{58}$$

where the vector $\tilde{\boldsymbol{b}}$ varies linearly in through-the-thickness direction such that:

$$\tilde{\boldsymbol{b}}\left(\xi^1,\xi^2,\zeta\right)=\zeta\boldsymbol{b}\left(\xi^1,\xi^2\right) \tag{59}$$

Note that $\boldsymbol{b}$ in Eq. (59) is still undefined. The enhancement (58) allows us to write the deformation gradient as:

$$\begin{aligned}\bar{\boldsymbol{F}}&=\boldsymbol{a}_\alpha\otimes\boldsymbol{g}^\alpha+\bar{\boldsymbol{a}}_3\otimes\boldsymbol{g}^3=\\&=\left(\left[\frac{\partial\boldsymbol{x}}{\partial\xi}\right]+\tilde{\boldsymbol{H}}\right)\left[\frac{\partial\boldsymbol{X}}{\partial\xi}\right]^{-1}=\left(\boldsymbol{J}+\tilde{\boldsymbol{H}}\right)\boldsymbol{J}_0^{-1}=\\&=\boldsymbol{F}+\tilde{\boldsymbol{F}}=\boldsymbol{a}_i\otimes\boldsymbol{g}^i+\tilde{\boldsymbol{b}}\otimes\boldsymbol{g}^3\end{aligned} \tag{60}$$

In Eq. (60) the natural coordinates are regrouped in a vector $\boldsymbol{\xi}=\left\{\xi^1,\xi^2,\xi\right\}^T$, $\boldsymbol{F}$ is the deformation gradient of the 6-parameter theory described in the previous section and $\tilde{\boldsymbol{F}}$ is an enhanced part of the deformation gradient due to an enhancement of the base vector. To simplify the notation we collected in Eq. (60) the base vectors of deformed and initial configurations into the following matrices (note that the usual simplifications carried out in the shell theory developments include also setting $\zeta=0$ when evaluating $\boldsymbol{J}_0$ (i.e. neglecting variation of metrics through the shell thickness in the initial configuration), which is not done in the present work):

$$\begin{aligned}&\boldsymbol{J}=\left[\boldsymbol{a}_1,\boldsymbol{a}_2,\boldsymbol{a}_3\right],\quad\tilde{\boldsymbol{H}}=\left[0,0,\tilde{\boldsymbol{b}}\right]\\&\boldsymbol{J}_0=\left[\boldsymbol{g}_1,\boldsymbol{g}_2,\boldsymbol{g}_3\right],\quad\boldsymbol{J}_0^{-T}=\left[\boldsymbol{g}^1,\boldsymbol{g}^2,\boldsymbol{g}^3\right]\end{aligned} \tag{61}$$

Note that $\boldsymbol{a}_i$ for the 6-parameter theory are defined in Eq. (34), while $\boldsymbol{g}_i$ are given in Eq. (16). The right Cauchy-Green stretch tensor:

$$\boldsymbol{C}=\bar{\boldsymbol{F}}^T\bar{\boldsymbol{F}}=\boldsymbol{J}_0^{-T}\left(\boldsymbol{J}+\tilde{\boldsymbol{H}}\right)^T\left(\boldsymbol{J}+\tilde{\boldsymbol{H}}\right)\boldsymbol{J}_0^{-1} \tag{62}$$

leads to the Green-Lagrange strains in $\boldsymbol{g}_i$ base $\boldsymbol{E}=\frac{1}{2}(\boldsymbol{C}-\boldsymbol{I})=E_{ij}\boldsymbol{g}^i\otimes\boldsymbol{g}^j$ according to:

$$\begin{aligned}E_{\alpha\beta}&=\frac{1}{2}\left(\boldsymbol{a}_\alpha\cdot\boldsymbol{a}_\beta-\boldsymbol{g}_\alpha\cdot\boldsymbol{g}_\beta\right)\\E_{\alpha3}&=\frac{1}{2}\left[\boldsymbol{a}_\alpha\cdot\left(\boldsymbol{d}+\tilde{\boldsymbol{b}}\right)-\underbrace{\boldsymbol{g}_\alpha\cdot\boldsymbol{g}_\beta}_{0}\right]=\frac{1}{2}\boldsymbol{a}_\alpha\cdot\boldsymbol{d}+\frac{1}{2}\boldsymbol{a}_\alpha\cdot\tilde{\boldsymbol{b}}\\E_{33}&=\frac{1}{2}\left[\left(\boldsymbol{d}+\tilde{\boldsymbol{b}}\right)\cdot\left(\boldsymbol{d}+\tilde{\boldsymbol{b}}\right)-\boldsymbol{g}_3\cdot\boldsymbol{g}_3\right]=\\&=\frac{1}{2}\left(\boldsymbol{d}\cdot\boldsymbol{d}-\boldsymbol{g}_3\cdot\boldsymbol{g}_3\right)+\frac{1}{2}\left(2\boldsymbol{d}\cdot\tilde{\boldsymbol{b}}+\tilde{\boldsymbol{b}}\cdot\tilde{\boldsymbol{b}}\right)\end{aligned} \tag{63}$$

We can conclude from Eq. (63) that:

$$E_{ij}=H_{ij}+\zeta K_{ij}+\zeta^2 L_{ij} \tag{64}$$

where H_{ij}, $K_{\alpha\beta}$ and $L_{\alpha\beta}$ strains are the same as those already given in Eqs. (37), (38) and (39), respectively, while other strains of the 6-parameter model from Section 3.1 are modified to be:

$$\begin{aligned}K_{\alpha3}&=\frac{1}{2}\left(\boldsymbol{d}_{,\alpha}\cdot\boldsymbol{d}+\boldsymbol{\varphi}_{,\alpha}\cdot\boldsymbol{b}\right)\\K_{33}&=\frac{1}{2}\left(2\boldsymbol{d}\cdot\boldsymbol{b}\right)\end{aligned} \tag{65}$$

$$\begin{aligned}L_{\alpha3}&=\frac{1}{2}\left(\boldsymbol{d}_{,\alpha}\cdot\boldsymbol{b}\right)\\L_{33}&=\frac{1}{2}\left(\boldsymbol{b}\cdot\boldsymbol{b}\right)\end{aligned} \tag{66}$$

Through-the-thickness variation of all strains is quadratic.

Note that one cannot use any more an additive split of the total strain, as in the previously described implementation. However, the admissible variations of the Green-Lagrange strains, Eq. (64), can still be written in terms of an additive decomposition as:

$$\delta E_{ij} + \delta \tilde{E}_{ij} \tag{67}$$

where:

$$\delta E_{ij} = \frac{1}{2}\left(\delta \boldsymbol{a}_i \cdot \boldsymbol{a}_j + \boldsymbol{a}_i \cdot \delta \boldsymbol{a}_j\right) \tag{68}$$

and:

$$\delta \tilde{E}_{ij} = \begin{cases} 0 & i,j = 1 \text{ or } 2 \\ \frac{1}{2}\left(\delta \boldsymbol{a}_\alpha \cdot \tilde{\boldsymbol{b}} + \boldsymbol{a}_\alpha \cdot \delta \tilde{\boldsymbol{b}}\right) & i \text{ or } j = 3 \\ \delta \boldsymbol{d} \cdot \tilde{\boldsymbol{b}} + \delta \tilde{\boldsymbol{b}} \cdot \boldsymbol{d} + \delta \tilde{\boldsymbol{b}} \cdot \tilde{\boldsymbol{b}} & i,j = 3 \end{cases} \tag{69}$$

The corresponding variational formulation can be obtained by generalizing the incompatible mode method of Ibrahimbegović and Frey, Ref. [3], from membranes to shells. To that end, two equations governing equilibrium can be written as:

$$\begin{aligned} & D\Pi\left(\underbrace{\varphi, a, \lambda}_{\boldsymbol{\Phi}}, \tilde{H}_i^j, P_i^j\right) \cdot \delta \boldsymbol{\Phi} = \\ & = \int_A \int_{h_0} \delta E_{ij} S^{ij} dV - D\Pi_{ext}(\varphi) \cdot \delta \varphi = 0 \end{aligned} \tag{70}$$

for the corresponding variation of the compatible displacement field and:

$$D\Pi\left(\boldsymbol{\Phi}, \tilde{H}_i^j, P_i^j\right) \cdot \delta \tilde{H}_i^j = \int_A \int_{h_0} \delta \tilde{E}_{ij} S^{ij} dV = 0 \tag{71}$$

for the incompatible mode variations. In Eqs. (70) and (71) we compute the second Piola-Kirchhoff stress from the constitutive equations for the first Piola-Kirchhoff stress, $P_i^j = \dfrac{\partial W}{\partial F_i^j}$, along with the geometric transformation connecting the two kinds of Piola-Kirchhoff stresses, $\boldsymbol{S} = \boldsymbol{F}^{-1}\boldsymbol{P}$. The last two equations have to be accompanied by an additional expression which guaranties the convergence of the incompatible mode method in the sense of the patch test, which can be written as:

$$\int_A \int_{h_0} \tilde{H}_i^j dV = 0 \tag{72}$$

In the finite element implementation we choose $\boldsymbol{b}$, see Eq. (59), to be:

$$\boldsymbol{b} = \boldsymbol{A}_{33}\boldsymbol{d} \tag{73}$$

where $\boldsymbol{d}$ is the extensible shell director already expressed in Eq. (10). From Eqs. (58) and (59) follows that the enhanced base vector at the deformed configuration is of the form:

$$\bar{\boldsymbol{a}}_3 = \left(1 + \zeta \boldsymbol{A}_{33}\right)\boldsymbol{d} \tag{74}$$

An interpolation of $\boldsymbol{A}_{33}$ over the finite element may be chosen again either by Eq. (48) or by standard bi-linear interpolation functions, Eq. (49). With this choice of interpolation, the patch test is naturally satisfied, which can be proved in the same manner as already shown in Eqs. (47) and (52).

4. INTERPOLATION AND FINITE ELEMENT IMPLEMENTATION

Finite element approximation of the shell models developed in the above sections is based on finite elements with four nodes on the middle surface. Convective coordinates ξ^1 and ξ^2 from previous sections are now replaced with isoparametric coordinates of a shell finite element. According to the isoparametric concept we use standard bi-linear interpolation functions to define middle surface geometry within one element as:

$$\varphi_0 = \sum_{a=1}^{n_{en}} N_a\left(\xi^1, \xi^2\right)\left(\varphi_0\right)_a, \quad \varphi = \sum_{a=1}^{n_{en}} N_a\left(\xi^1, \xi^2\right)\varphi_a \tag{75}$$

where the number of element nodes n_{en}=4, $N_a : \square \rightarrow \square$ are the corresponding shape functions already given in Eq. (51), whereas $(o)_a$ are the corresponding nodal values. Through-the-thickness kinematic variables are interpolated in the same manner:

$$\tilde{\lambda} = \sum_{a=1}^{n_{en}} N_a \tilde{\lambda}_a, \quad \tilde{\lambda} = 1 - \lambda \tag{76}$$

$$q = \sum_{a=1}^{n_{en}} N_a q_a \tag{77}$$

It is indicated in Eq. (76) that rather than the thickness-change variable λ we interpolate $\tilde{\lambda}$ in order to have zero values of all unknown kinematic variables at the initial configuration. Current thickness is then expressed as:

$$h = h_0\left(1 - \tilde{\lambda}\right), \quad \tilde{\lambda} \le 1 \tag{78}$$

Approximation of the shell director requires special attention in order to obtain good numerical performance of the 6- and the 7-parameter models for very thin shells. Very often parasitic through-the-thickness strains are induced through a simple interpolation of the shell director, especially in formulations where rotations are avoided by introducing the so-called difference vector (Refs. [4, 7]). In some works the effect of artificial thickness strains is avoided by assumed strain approximation of E_{33} (Ref. [25]). To avoid this approximation in the present work, the shell director is normalized over an element in order to always remain exactly of a unit length at the integration points:

$$\boldsymbol{a}=\frac{\hat{\boldsymbol{a}}}{\|\hat{\boldsymbol{a}}\|},\quad \hat{\boldsymbol{a}}=\sum_{a=1}^{n_{en}} N_a \boldsymbol{a}_a \tag{79}$$

$$\boldsymbol{g}=\frac{\hat{\boldsymbol{g}}}{\|\hat{\boldsymbol{g}}\|},\quad \hat{\boldsymbol{g}}=\sum_{a=1}^{n_{en}} N_a \boldsymbol{g}_a \tag{80}$$

The nodal shell director in a deformed configuration is given as a function of the total nodal material rotation vector $\vartheta_a=\left\{\vartheta_a^1,\vartheta_a^2\right\}^T$ with (see Ref. [21]):

$$\boldsymbol{a}_a=\Lambda_{0a}\left(\cos\vartheta_a\left\{0,0,1\right\}^T+\frac{\sin\vartheta_a}{\vartheta_a}\left\{\vartheta_a^2,-\vartheta_a^1,0\right\}^T\right) \tag{81}$$

where $\vartheta_a=\|\vartheta_a\|$ is the Euclidean norm of the nodal rotation vector and $\Lambda_{0a}=\left[\boldsymbol{e}_{1a},\boldsymbol{e}_{2a},\boldsymbol{g}_a\right]$ is the initial nodal rotation matrix providing orientation for the nodal rotation parameters ϑ_a^1 and ϑ_a^2. Vectors $\boldsymbol{e}_{1a}$, $\boldsymbol{e}_{2a}$ and $\boldsymbol{g}_a$ define Cartesian basis at node a.

The virtual and the incremental quantities are interpolated as:

$$\delta\varphi=\sum_{a=1}^{n_{en}} N_a\varphi_a,\quad \delta\tilde{\lambda}=\sum_{a=1}^{n_{en}} N_a\tilde{\lambda}_a,\quad \delta q=\sum_{a=1}^{n_{en}} N_a q_a \tag{82}$$

$$\delta\boldsymbol{a}=\frac{1}{\|\hat{\boldsymbol{a}}\|}\left(\boldsymbol{I}-\boldsymbol{a}\otimes\boldsymbol{a}\right)\delta\hat{\boldsymbol{a}},\quad \delta\hat{\boldsymbol{a}}=\sum_{a=1}^{n_{en}} N_a\delta\boldsymbol{a}_a \tag{83}$$

Derivatives of the interpolated quantities with respect to ξ^α coordinates can be obtained trivially except for $\boldsymbol{a}_{,\alpha}$ and $\delta\boldsymbol{a}_{,\alpha}$. Linearized quantities $\Delta\delta\boldsymbol{a}$ and $\Delta\delta\boldsymbol{a}_{,\alpha}$ have even more complicated forms and can be mainly obtained by using symbolic manipulations.

In order to eliminate the shear locking effect, the transverse shear strains are interpolated over a parent element by using the assumed natural strain (ANS) concept of Bathe and Dvorkin in Ref. [26] according to:

$$\begin{aligned}\bar{E}_{13}&=\frac{1}{2}\left[\left(1-\xi^2\right)E_{13}^B+\left(1+\xi^2\right)E_{13}^D\right]\\ \bar{E}_{23}&=\frac{1}{2}\left[\left(1-\xi^1\right)E_{23}^A+\left(1+\xi^1\right)E_{23}^C\right]\end{aligned} \tag{84}$$

Strains $E_{i3}^{(o)}$ are evaluated at the mid-side point (o) in accordance with the expressions derived in the previous sections. Linear and higher order terms of $E_{i3}^{(o)}$ are automatically neglected by choosing the shear interpolation points A, B, C and D on the middle surface of the shell finite element corresponding to $\zeta=0$. Positions of those points are $\varphi_0^L=\frac{1}{2}\left[\left(\varphi_0\right)_M+\left(\varphi_0\right)_N\right]$, where $(L,M,N)\in\{(A,1,2),(B,2,3),(C,3,4),(D,l,4)\}$. Finite element approximation of the transverse shear strains across the thickness of the shell element is therefore assumed to be constant.

Numerical integration is performed at $2\times2\times2$ Gauss integration points. At each integration point a local Cartesian basis e_i is introduced in such a way that the third base vector is identical to the initial shell director and the other two are perpendicular to it:

$$\boldsymbol{e}_3=\boldsymbol{g},\quad \boldsymbol{e}_1\perp\boldsymbol{e}_2,\quad \boldsymbol{e}_1\times\boldsymbol{e}_2=\boldsymbol{e}_3 \tag{85}$$

Having defined the current and the initial position vectors over a finite element domain, we may obtain the deformation gradient at an integration point as:

$$\boldsymbol{F}=\frac{\partial\boldsymbol{x}}{\partial\boldsymbol{x}_0}=\left[\frac{\partial\boldsymbol{x}}{\partial\xi}\right]\left[\frac{\partial\boldsymbol{x}_0}{\partial\xi}\right]^{-1}=\boldsymbol{J}\boldsymbol{J}_0^{-1} \tag{86}$$

where $\boldsymbol{J}$ and $\boldsymbol{J}_0$ are defined in Eq. (61). The right Cauchy-Green stretch tensor can be computed from the deformation gradients (we note again that the deformation gradient is enriched for the method described in Section 3.2, see (Eq. 60); in that case we use Eq. (62) instead of Eq. (87)) as:

$$\boldsymbol{C}=\boldsymbol{F}^T\boldsymbol{F}=\boldsymbol{J}_0^{-T}\left(\boldsymbol{J}^T\boldsymbol{J}\right)\boldsymbol{J}_0^{-1}=C_{ij}\boldsymbol{g}^i\otimes\boldsymbol{g}^j \tag{87}$$

where the corresponding components in the $\boldsymbol{g}_i$ basis are $C_{ij}=\boldsymbol{a}_i\cdot\boldsymbol{a}_j=\boldsymbol{J}^T\boldsymbol{J}$. The transformation of C_{ij} components to the C^*_{ij} components, which are defined with respect to the $\boldsymbol{e}_i$ basis, Eq. (85), can be performed according to:

$$\begin{aligned}\left[C_{ij}^*\right]&=\left[\boldsymbol{e}_1,\boldsymbol{e}_2,\boldsymbol{g}\right]^T\boldsymbol{J}_0^{-T}\left[C_{ij}\right]\boldsymbol{J}_0^{-1}\left[\boldsymbol{e}_1,\boldsymbol{e}_2,\boldsymbol{g}\right]=\\ &=\boldsymbol{T}\left[C_{ij}\right]\boldsymbol{T}^T\end{aligned} \tag{88}$$

where the transformation matrix has the following form:

$$\boldsymbol{T}=\begin{bmatrix}\boldsymbol{g}^1\cdot\boldsymbol{e}_1 & \boldsymbol{g}^2\cdot\boldsymbol{e}_1 & 0\\ \boldsymbol{g}^1\cdot\boldsymbol{e}_2 & \boldsymbol{g}^2\cdot\boldsymbol{e}_2 & 0\\ 0 & 0 & \dfrac{2}{h_0}\end{bmatrix} \tag{89}$$

Strains in the local Cartesian frame, Eq. (85), can then be calculated as:

$$E_{ij}^*=\frac{1}{2}\left(C_{ij}^*-\delta_{ij}\right) \tag{90}$$

The transformation of the transverse shear strains from the ξ coordinates to the local Cartesian coordinates defined with basis $\boldsymbol{e}_i$, Eq. (85), is performed as [27]:

$$\begin{Bmatrix}E_{13}^*\\ E_{23}^*\end{Bmatrix}=\begin{bmatrix}\boldsymbol{g}_1\cdot\boldsymbol{e}_1 & \boldsymbol{g}_1\cdot\boldsymbol{e}_2\\ \boldsymbol{g}_2\cdot\boldsymbol{e}_1 & \boldsymbol{g}_2\cdot\boldsymbol{e}_2\end{bmatrix}^{-1}\frac{2}{h_0}\begin{Bmatrix}\hat{E}_{13}\\ \hat{E}_{23}\end{Bmatrix} \tag{91}$$

where an additional term $2/h_0$ appears due to the definition of ζ coordinate which leads to the base vectors $\boldsymbol{g}_3=\frac{h_0}{2}\boldsymbol{g}$ and $\boldsymbol{g}^3=\frac{2}{h_0}\boldsymbol{g}$.

With Eqs. (90) and (91) we can define the potential energy of the shell in terms of E_{ij}^* strains. Symbolic manipulation (see Ref. [24]) is further used to obtain its first and second derivative with respect to the nodal unknown kinematic variables leading to residuals and stiffness matrix. When internal variables are present, the final form of the stiffness matrix is obtained by the procedure of static condensation.

5. NUMERICAL EXAMPLES

In this section we present some results of numerical simulations. The computations were carried out by a research version of the computer program AceGen (see Ref. [24]). We have implemented the following 4-node finite elements listed in Table 1: five for the St. Venant-Kirchhoff (SVK) material and four for the neo-Hookean (NH) material with a strain energy function of the form given by Eq. (25). For the 5-parameter SVK element we condensed 3D constitutive relations by using the condition $S_{33}=0$. In all examples we used $2\times2\times2$ Gaussian integration rule. A tolerance of 10^{-9} for the Euclidean norm of iterative nodal values was employed in the Newton iteration scheme for each of the examples.

Table 1 Finite elements used in numerical examples

5E	5-parameter model with exact (E) strains
7E	7-parameter model with exact (E) strains; see Eq. (17)
7R	7-parameter model with reduced (R) strains; see Eq. (23)
6EA	6-parameter model with exact (E) strains an incompatible mode based on an additive (A) decomposition of strains; interpolation, Eq. (48)
6EM	6-parameter model with exact (E) strains and incompatible mode based on a. multiplicative (M) decomposition of strains; interpolation, Eq. (48)

5.1 Bending of a strip by end force

This example demonstrates the ability of finite elements based on non-standard theories to recover 2D shell behavior in the thin shell limit. We consider a strip of length $L=10$, width $B=1$ and thickness h_0, which is clamped at one end and subjected to two point forces $F=F_1=40\times10^3\times h_0^3$ acting on the middle surface of the free end (see Figure la). Four different values (2, *1*, *0.1*, *0.01*) are used for thickness producing length-to-thickness ratios to be *5*, *10*, *100* and *1000*. Material parameters are $E=10\times10^6$, $\nu=0.3$. A mesh of 10×1 element is used. We present results of the nonlinear analyses.

The free end deflections, produced by different elements, are given in Tables 2 and 3. It can be observed from Tables 2 and 3 that in the thin shell limit, ($L/h_0=1000$) the elements 5E, 6AD and 6MD produce identical results, which indicates that formulations based on incompatible modes recover the thin shell solution, while elements based on the 7-parameter theory (7E and 7R) produce approximately *99%* of the 5E element results. It can be also observed that the difference between the 7E and the 9R solutions increases with decreasing L/h_0 ratio, which suggests that the higher order strain terms are more important for thicker shells. The same is valid for incompatible mode formulations: the difference in results increases with increase of thickness. In Table 4 we collect maximum values of $\tilde{\lambda}$ at the points with maximum curvatures. Those values are small: maximum thickness change is around *3%* for beams with $L/h_0=5$. Distribution of $\tilde{\lambda}$ through the beam length is shown in Figure 1b.

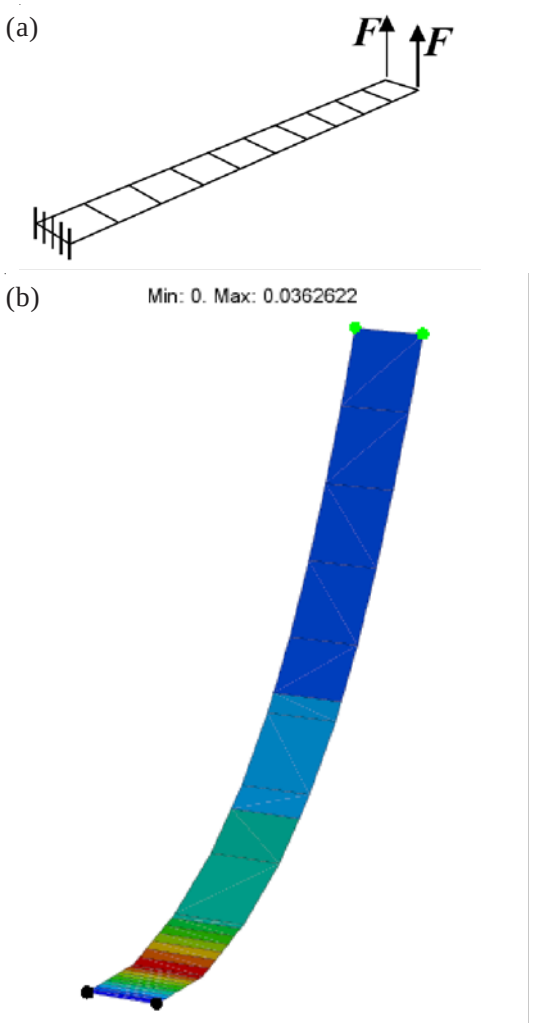

Fig. 1 Bending of a strip by end force: (a) finite element mesh and loading; (b) stretch distribution in final deformed configuration

Table 2 Bending of a strip by end force; end deflection at $F=F_1$; SVK material

L/h_0	5	10	100	1000
Element/ Material	SVK	SVK	SVK	SVK
5E	7.3492	7.1188	7.0477	7.0470
7E	7.3037	7.0568	6.9869	6.9874
7R	7.2624	7.0453	6.9868	6.9874
6EA	7.3797	7.1278	7.0477	7.0470
6EM	7.3867	7.1294	7.0478	7.0470

Table 3 Bending of a strip by end force; end deflection at $F=F_1$; NH material

L/h_0	5	10	100	1000
Element/ Material	NH	NH	NH	NH
7E	7.3404	7.0691	6.9870	6.9874
7R	7.3083	7.0586	6.9869	6.9874
6EA	7.4146	7.1401	7.0479	7.0467
6EM	7.4184	7.1411	7.0479	7.0467

Table 4 Bending of a strip by end force; maximum values of $\tilde{\lambda}$ (at the point of maximum curvature) multiplied by 100 at $F=F_1$; SVK material

Element/L/h_0	5	10	100
7E	2.847	0.580	0.005
7R	3.626	0.790	0.007
6EA	3.154	0.772	0.008
6EM	2.389	0.804	0.008

In Table 5 we present the total number of iterations when the forces $F=F_1$ are applied in five equal increments. It is interesting to note that the number of iterations depends only on the length-to-thickness ratio.

Table 5 Bending of a strip by end force: total number of iterations; $F=F_1$; SVK material

Element/L/h_0	5	10	100	1000
5E	34	37	50	62
7E	34	37	50	63
7R	34	37	50	63
6EA	34	37	51	63
6EM	34	37	51	63

5.2 Cylinder under line load

In this example we consider a cylinder under line distributed loading, in order to test the behavior of 3D shell formulations for thick shell applications. The cylinder of length $L=30$ *cm*, radius $R=9$ *cm* and thickness $h_0=(0.2\ cm,\ 2\ cm)$ is supported and subjected to a line load p as shown in Figure 2a. Due to symmetry conditions only one quarter of the cylinder is discretized by 16×6 4-node finite elements. The parameters of the neo-Hookean material are $\mu=6000\ kN/cm^2$, $\lambda=24000\ kN/cm^2$ or $E=16800\ kN/cm^2$, $\nu=0.4$. The load, which is acting on the middle surface, was applied in five equal steps.

In Table 6 we compare our results with those given by Buchter, Ramm and Roehl [7], who used a mesh of 16×6 8-node elements with $2\times2\times3$ Gauss integration points. Comparison is carried out for a total load when the displacement of the point under the force at the free edge (point A) equals to *16 cm*. The response curves for all elements are very similar when it comes to computed displacement values. In Figure 2b we plotted the distribution of thickness change. Maximum values of about *4%* are at the free end of the shell (at the region of maximum curvature) and at the point A. The thickness stretch of the point A with respect to the total load is presented in Figures 3a and 3b for SVK and NH material models. We note that the multiplicative decomposition based incompatible modes seem to be advantageous over the additive decomposition in the region of a large thickness change.

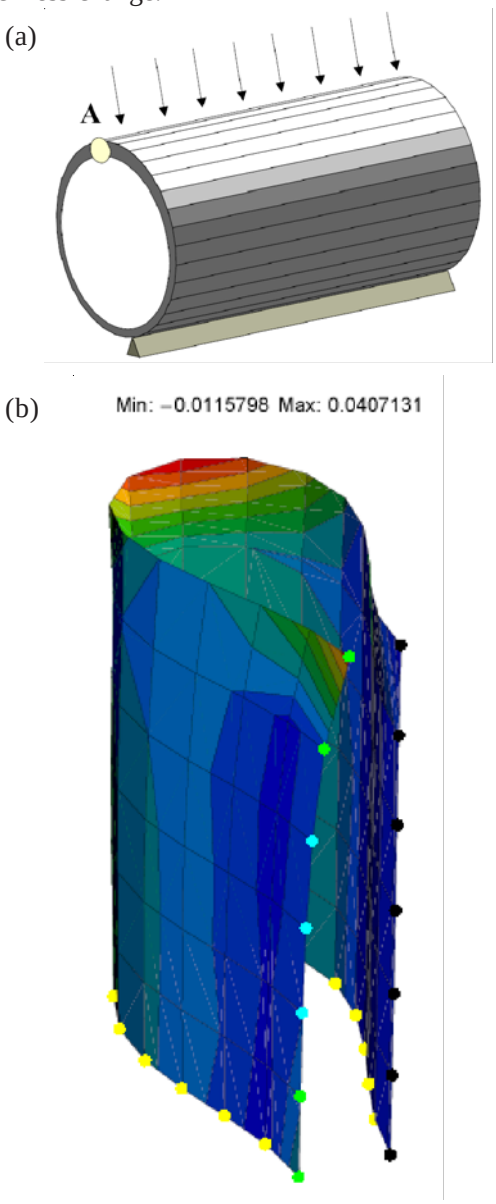

Fig. 2 Cylinder under line load: (a) finite element mesh and loading; (b) stretch distribution in final deformed configuration

Table 6 Hyperelastic cylinder; total load [kN] when displacement of point A is 16 cm: 16×6 elements

(Element, Material) / h_0	0.2 cm	2 cm
5E, SVK	35.13	28961
7E, SVK	35.43	28561
7R, SVK	35.46	30027
6EA, SVK	35.12	28935
6EM, SVK	35.13	28706
7E, NH	35.47	29445
7R, NH	35.49	30805
6EA, NH	35.12	29731
6EM, NH	35.13	29530
7E, NH, Ref. [11]	34.71	28636
7R, NH, Ref. [11]	34.70	28428
6EA, NH, Ref. [11]	34.71	29984
6EM, NH, Ref. [11]	34.87	33680

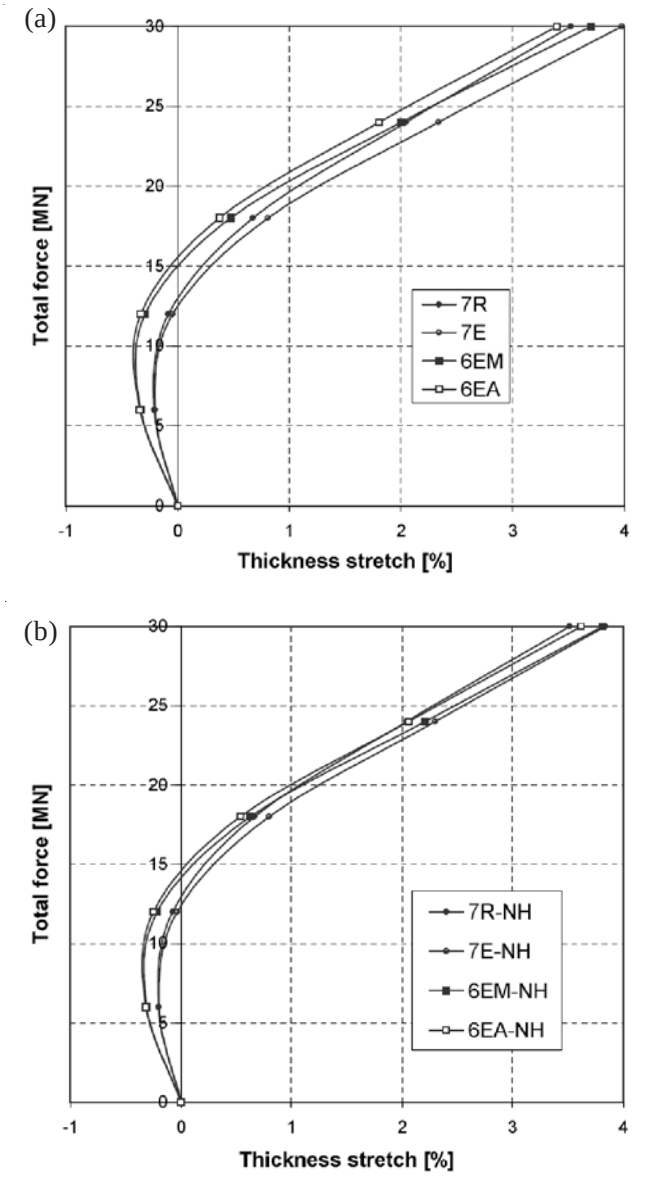

Fig. 3 Cylinder under line load: thickness change at point A for: (a) SVK models and (b) NH models

6. CONCLUSIONS

Three nonlinear shell formulations accounting for through-the-thickness stretching were developed, one leading to a 7-parameter theory and the other two to theories with 6 parameters. All developed finite elements posses three displacement degrees of freedom and two rotations, and each one is capable of representing a linear variation of the through-the-thickness strain.

The 7-parameter shell theory is developed and tested in its full generality before reducing it to the usual format where only linear through-the-thickness variations of strain measures are kept. This kind of development is relatively easy to handle by symbolic manipulation. An incompatible mode method is used to reduce the 7-parameter shell theory to the one with only 6 nodal parameters, which is easier to implement within the standard finite element computer program architecture.

The main advantage of all presented shell models relates to a possibility to employ directly a 3D form of constitutive equations with no presence of locking phenomena. Additional cures for locking employed by the derived elements include the assumed natural strain (ANS) method for the transverse shear locking, and the exact director vector interpolation for the curvature locking.

In the thin shell limit the elements with incompatible modes produce the same results as those obtained by the classical shell elements based on the Reissner-Mindlin kinematics (for the chosen numerical examples); i.e. the enhancement on through-the-thickness strain is not activated if not needed. The same is no longer true for the 7-parameter models which will not necessarily yield the same results as the 5-parameter model. For thick shells, the numerical results show that the influence of higher order strains (which are usually neglected in shell theories) increases. In the computed examples there were no significant differences between two incompatible modes methods (one with an additive decomposition of strains and another with a multiplicative decomposition of strains) if thickness change was not extremely significant. The loading was applied at the shell middle surface in all numerical examples, however, the results indicate that the influence of the loading position to local results is quite important.

ACKNOWLEDGEMENTS

This collaboration was supported by French-Slovenian collaboration program PROTEUS. Adnan Ibrahimbegovic would also like to acknowledge the Slovenian Research Agency Award for foreign scientists in 2007.

7. REFERENCES

[1] A. Ibrahimbegović and B. Brank, Shell model representation for finite rotations and finite strains, Proc. of Special Workshop on Advanced Nuerical Analysis of Shell-like Structures, Eds. J. Sorić, F. Gruttmann and W. Wagner, Zagreb, September 2007., Croatian Society of Mechanics, Zagreb, pp. 31-51, 2007.

[2] P.M. Naghdi, The theory of shells and plates, in: S. Flugge (ed.), *Encyclopedia of Physics*, Springer-Verlag, 1972.

[3] A. Ibrahimbegović, Stress resultant geometrically exact shell theory for finite rotations and its finite element implementation, *Appl. Mech. Rev.*, Vol. 50, pp. 199-226, 1997.

[4] J.C. Shoo, M.S. Rifai and D.D. Fox, On a stress resultant geometrically exact shell model - Part IV: Variable thickness shells with through-the-thickness stretching, *Comput. Methods Appl. Mech. Engrg.*, Vol. 81, pp. 91-126, 1990.

[5] P. Betsch, F. Gruttmann and E. Stein, A 4-node finite shell element for the implementation of general hyperelastic 3D-elasticity at finite strains, *Comput. Methods Appl. Mech. Engrg.*, Vol. 130, pp. 57-79, 1996.

[6] Y. Bagar, M. Itskov and A. Eckstein, Composite laminates: Nonlinear interlaminar stress analysis by multi-layer shell elements, *Comput. Methods Appl. Mech. Engrg.*, Vol. 185, pp. 367-397, 2000.

[7] N. Buchter, E. Ramm and D. Roehl, Three-dimensional extension of nonlinear shell formulation based on the enhanced assumed strain concept, *Int. J. Numer. Methods Engng.*, Vol. 37, pp. 2551-2568, 1994.

[8] M. Bischoff and E. Ramm, Shear deformable shell elements for large strains and rotations, *Int. J. Numer. Methods Engng.*, Vol. 40, pp. 4427-4449, 1997.

[9] C. Sansour, A theory and finite element formulation of shells at finite deformations involving thickness change: Circumventing the use of a rotation tensor, *Archive of Applied Mechanics*, Vol. 65, pp. 194-216, 1995.

[10] H. Parisch, A continuum-based shell theory for non-linear applications, *Int. J. Numer. Methods Engng.*, Vol. 38, pp. 1855-1883, 1995.

[11] S. Klinkel, F. Gruttmann and W. Wagner, A continuum based three-dimensional shell element for laminated structures, *Computers and Structures*, Vol. 71, pp. 43-62, 1999.

[12] R. Hauptmann, S. Doll, M. Harnau and K. Schweizerhof, 'Solid-shell' elements with linear and quadratic shape functions at large deformations with nearly incompressible materials, *Computers and Structures*, Vol. 79, pp. 1671-1685, 2001.

[13] J.C. Simo, D.D. Fox and M.S. Rifai, A class of mixed assumed strain methods and the method of incompatible modes, *Int. J. Numer. Methods Engng.*, Vol. 29, pp. 1595-1638, 1990.

[14] A. Ibrahimbegović and E.I. Wilson, A modified method of incompatible modes, *Commun. Numer. Methods Engng.*, Vol. 8, pp. 23-32, 1991.

[15] A. Ibrahimbegović and F. Frey, Geometrically non-linear method of incompatible modes in application to finite elasticity with independent rotations, *Int. J. Numer. Methods Engng.*, Vol. 36, pp. 4185-4200, 1993.

[16] W.B. Kratzig, "Best" transverse shearing and stretching shell theory for nonlinear finite element simulations, *Comput. Methods Appl. Mech. Engrg.*, Vol. 103, pp. 135-160, 1993.

[17] A. Ibrahimbegović, B. Brank and P. Courtois, Stress resultant geometrically exact form of classical shell model and vector-like parametrization of constrained finite rotations, *Int. J. Numer. Methods Engng.*, Vol. 52, pp. 1235-1252, 2001.

[18] B. Brank and A. Ibrahimbegović, On the relation between different parametrizations of finite rotations for shells, *Engineering Computations*, Vol. 18, pp. 950-973, 2001.

[19] J.C. Simo, M.S. Rifai and D.D. Fox, On a stress resultant geometrically exact shell model - Part III: Computational aspects of the nonlinear theory, *Comput. Methods Appl. Mech. Engrg.*, Vol. 79, pp. 21-70, 1990.

[20] N. Buchter and E. Ramm, Shell theory versus degeneration - a comparison in large rotation finite element analysis, *Int. J. Numer. Methods Engng.*, Vol. 34, pp. 39-59, 1992.

[21] B. Brank, D. Perić and F.B. Damjanić, On large deformations of thin elasto-plastic shells: Implementation of a finite rotation model for quadrilateral shell element, *Int. J. Numer. Methods Engng.*, Vol. 40, pp. 689-726, 1997.

[22] O.C. Zienkiewicz and R.L. Taylor, *The Finite Element Method: Basic Formulation and Linear Problems*, Vol. 1, McGraw-Hill, 1989.

[23] M. Bischoff and E. Ramm, On the physical significance of higher order kinematic and static variables in a three-dimensional shell formulation, *Int. Journal of Solids and Structures*, Vol. 37, pp. 6933-6960, 2000.

[24] J. Korelc, Automatic generation of finite element code by simultaneous optimization of expressions, *Theor. Comput. Sci.*, Vol. 187, pp. 231-248, 1997.

[25] P. Betsch and E. Stein, An assumed strain approach avoiding artificial thickness straining for a non-linear 4-node shell element, *Commun. Numer. Methods Engng.*, Vol. 11, pp. 899-909, 1995.

[26] K.J. Bathe and E. Dvorkin, A four-node plate bending element based on Mindlin-Reissner plate theory and a mixed interpolation, *Int. J. Numer. Methods Engng.*, Vol. 21, pp. 367-383, 1985.

[27] A. Ibrahimbegović, On assumed shear strain in finite rotation shell analysis, *Engineering Computations*, Vol. 12, pp. 425-438, 1995.

SUVREMENA DOSTIGNUĆA U NELINEARNOJ TEORIJI LJUSKI S KONAČNIM ROTACIJAMA I KONAČNIM DEFORMACIJAMA

SAŽETAK

U ovom članku se analizira teorijska formulacija modela potpuno nelinearne ljuske koji može opisati konačne rotacije i konačne deformacije. Ovo drugo nam nameće ideju da treba uzeti u obzir deformacije koje se protežu cijelom debljinom što omogućava direktno korištenje trodimenzionalnih konstitutivnih jednadžbi iz klasičnog modela kontinuuma. Ispitane su tri različite mogućnosti primjene ovog modela ljuske pomoću metode konačnih elemenata. Prva mogućnost upućuje na sedam čvornih parametara, a preostale dvije mogućnosti na šest čvornih parametara. Sedam-parametarski model ljuske bez pojednostavljenja kinematičkih izraza uspoređuje se sa sedam-parametarskim modelom ljuske koji koristi uobičajena pojednostavljenja Green-Lagrangeovih deformacija. Ovdje su predstavljena dva različita načina primjene metode inkompatibilnih modova s ciljem da se smanji broj parametara na šest. Jedna primjena koristi dodatno rastavljanje deformacije, a druga dodatno rastavljanje gradijenta deformacije. Prikazano je nekoliko numeričkih primjera za ilustriranje ponašanja razvijenih elemenata ljuske.

***Ključne riječi**: ljuska, nelinearni model ljuske, konačne rotacije, konačne deformacije, adaptivna dekompozicija.*